What Fine-Tuning Changes: A Radiomic Lens on Prostate Foundation Model Representations

Yipei Wang[1] YIPEI.WANG@UCL.AC.UK
[1] *UCL Hawkes Institute, Department of Medical Physics and Biomedical Engineering, University College London*

Yaxi Chen[1] YAXI.CHEN.20@UCL.AC.UK
Wen Yan[1] WEN-YAN@UCL.AC.UK
Natasha Thorley[2,3] NATASHA.THORLEY@UCL.AC.UK
[2] *Centre for Medical Imaging, University College London*
[3] *Department of Radiology, University College London Hospital NHS Foundation Trust*

Alexander Ng[4] ALEXANDER.NG@UCL.AC.UK
[4] *Centre for Urology Imaging, Prostate, AI and Surgical Studies (COMPASS) Research Group, Division of Surgery and Interventional Science, University College London*

Dean C. Barratt[1] D.BARRATT@UCL.AC.UK

Daniel C. Alexander[1,5] D.ALEXANDER@UCL.AC.UK
[5] *Department of Computer Science, University College London*

Shonit Punwani[2,3] S.PUNWANI@UCL.AC.UK

Mark Emberton[6,7] M.EMBERTON@UCL.AC.UK
[6] *Department of Urology, University College London Hospital*
[7] *Division of Surgery and Interventional Science, University College London*

Veeru Kasivisvanathan[4,6] VEERU.KASI@UCL.AC.UK

Yipeng Hu[1] YIPENG.HU@UCL.AC.UK

Editors: Under Review for MIDL 2026

Abstract

Clarifying how foundation model encoders change during fine-tuning is important for transparency and trustworthiness in their medical imaging applications. It may also be useful for further understanding, developing and adapting these models. However, the latent representations produced by such encoders are high dimensional and lack explicit semantic meaning, making it difficult to characterise how task-specific adaptation modifies them. In this study, we introduce a radiomics-based framework that provides an interpretable lens through which these representational changes can be examined and often better understood. Using prostate cancer patient imaging data, we train a two-layer MLP to learn the relationship between radiomic descriptors and encoder embeddings prior to fine-tuning. This model

captures non-linear associations through its first layer, while the final linear layer offers an interpretable mapping from radiomic attributes to (transformed) latent features. To quantify the effect of fine-tuning, the first layer is fixed, and only the linear layer is re-estimated using the embeddings from the fine-tuned encoder. Comparing the pre- and post-fine-tuning linear weights yields a direct quantitative measure of how the encoder's emphasis on specific radiomic characteristics shifts during fine-tuning. We validate the approach using a prostate MRI foundation model and multiple downstream tasks. The analysis reveals consistent, task-dependent changes in the encoder's sensitivity to radiomic texture and intensity features. This work provides the first radiomics-based methodology for systematically interpreting how fine-tuning restructures foundation model representation in medical imaging. The implementation is available at: https://github.com/pipiwang/RaiomicLens

Keywords: mpMRI, Foundation model, Radiomic feature, Interpretability

1. Introduction

Foundation models which are pre-trained on large-scale datasets, often using a self-supervised learning paradigm, have increasingly been applied to medical related tasks on various modalities and anatomical structures (Wu et al., 2025; Zhou et al., 2023; Fu et al., 2025; Zhang et al., 2024; McConnell et al., 2025). These recent advances demonstrated the potential of foundation models of achieving better performance for individual applications when being fine-tuned and adapted to specific downstream tasks. However, current research has been largely motivated by and emphasising performance boosts over existing specialised supervised learning models, whereas the interpretability study on foundation models in medical applications is restricted to saliency maps (Zhou et al., 2023) or effects on quantitative results of different fine-tuning strategies (McConnell et al., 2025). The role of fine-tuning in affecting model behaviour and reshaping representation space in foundation models for medical tasks remains insufficiently studied.

Understanding how foundation model encoders change during fine-tuning is essential for interpreting their behaviour in medical image analysis. Although fine-tuning is known to adapt representations towards a target task, the nature of this adaptation is often opaque. Encoder features are high dimensional and lack clear semantic meaning, which makes it difficult to understand what prior knowledge is retained, what is modified, and how these changes relate to clinically meaningful image characteristics.

Radiomics provides a complementary, interpretable representation of medical images, consisting of comprehensive descriptions such as texture, intensity statistics and shape descriptors, for a given region of interest (ROI) (Zwanenburg et al., 2016; Aguirre-Meneses et al., 2025). These features provide quantitative characterisations of medical images which contribute to radiologists' decision-making process on disease diagnosis and treatment planning (Tomaszewski and Gillies, 2021). Unlike the obscure, high-dimensional features from deep learning models, radiomic features have explicit definitions that allow fine-grained interpretation. In this work, we propose to use radiomic features as an interpretable reference space to analyse how a foundation model encoder changes before and after fine-tuning.

This work proposes to model the relationship between radiomic features and encoder embeddings using a two-layer MLP. The network is first trained on the pre-fine-tuning encoder features so that it can learn a general non-linear mapping while keeping the final linear layer directly interpretable. To analyse how fine-tuning alters the encoder represen-

tation, we freeze the first layer of the MLP and solve the interpretation linear head using the fine-tuned embeddings. Comparing the two linear heads then highlights how the influence of each radiomic attribute has changed, offering an interpretable view of the effects of fine-tuning.

In this work, we introduce radiomics as an interpretable framework for explaining encoder representations on real patient medical imaging data. We provide the first radiomics-based analysis that makes encoder changes during fine-tuning quantitatively interpretable. The proposed approach is demonstrated using a prostate MRI foundation model across multiple downstream tasks, showing how radiomics reveals task-specific adaptation.

2. Method

We introduce a two-stage framework to investigate the relationship between the internal feature representation from the foundation model and radiomic features calculated directly from images, and capture the changes during task-specific fine-tuning, as shown in Fig. 1. At the first stage, features of the foundation model encoder from before and after fine-tuning are projected into a unified, non-linear space; while in the second stage, closed-form linear regression is applied to reconstruct radiomic features from the projected features. By analysing the difference of weights and residuals in the linear decoding between pre- and post- fine-tuning, we provide quantitative measures of representation shift during the fine-tuning process.

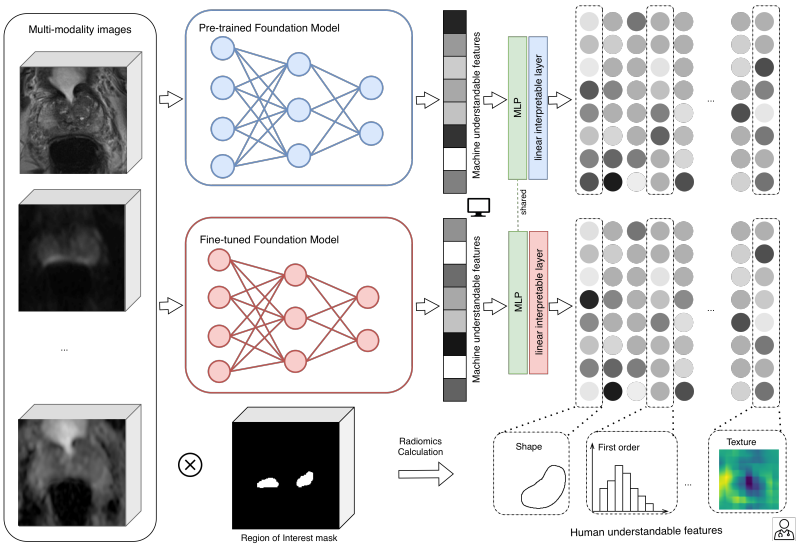

Figure 1: Overview of the proposed framework.

2.1. Problem formulation

Let $E(\cdot)$ denote a pre-trained foundation model encoder and $E_{ft}(\cdot)$ as one of its fine-tuned variants for a specific downstream task, which both map the input patient data x into a

d-dimensional feature space. For each patient data x, $X^{pre} = E(x)$ and $X^{ft} = E^{ft}(x)$, where $X^{pre} \in \mathbb{R}^d$ and $X^{ft} \in \mathbb{R}^d$ represent the features from the pre-trained and fine-tuned foundation model encoder respectively.

For each patient data x, there may exist more than one data modality, for example, various image modality sequences for multi-parametric magnetic resonance imaging (mpMRI). Radiomic features are calculated for each image modality m and the ROI pair, denoted as $R_m \in \mathbb{R}^n, m = 1, 2, ..., M$, where M denotes the total number of modalities of each patient. A set of radiomic features of the same types is calculated for each modality, resulting in M n-dimensional vectors, $R = [R_1^\intercal, R_2^\intercal, .., R_M^\intercal]^\intercal \in \mathbb{R}^{nM}$.

The goal is to establish a function

$$f : \mathbb{R}^d \to \mathbb{R}^{nM}, \tag{1}$$

that project the foundation model encoder features to the corresponding radiomic features.

2.2. Shared non-linear projection

We first project encoder features into a shared hidden space by learning a shared non-linear function,

$$Z = f^{share}(X; \phi) \tag{2}$$

In order to learn this projection, decompose f into a shared non-linear projection and modality-specific linear heads, denoted as:

$$f(X) = f^{head}(f^{share}(X; \phi), \theta). \tag{3}$$

The model parameters are optimised using L1 reconstruction loss with optional L_1, L_2, or elastic penalites on model weights:

$$\mathcal{L} = \mathcal{L}_{rec} + \lambda_1 ||\phi, \theta||_1 + \lambda ||\phi, \theta||_2^2. \tag{4}$$

Therefore,

$$(\hat{\phi}, \hat{\theta}) = \arg\min_{\phi,\theta} \sum_{m=1}^{M} ||f_m^{head}((f^{share}(X^{pre}, \phi); \theta_m) - R_m||_1 + \lambda_1 ||\phi, \theta||_1 + \lambda ||\phi, \theta||_2^2). \tag{5}$$

The first stage is optimised using features from before fine-tuning as input. Once trained, we freeze the weights of the shared function and discard the temporary heads f_m^{head}. The latent features obtained from this stage are denoted as $Z^p = f^{share}(X^{pre}; \hat{\phi})$ and $Z^{ft} = f^{share}(X^{ft}; \hat{\phi})$.

2.3. Closed-form linear radiomic decoding

After transforming the features from foundation models to the shared hidden space, we solve a new linear decoder for hidden features from pre- and post- fine-tuning separately using least-squares, in a single matrix form: $R = \theta Z$. The optimal parameters are solved by: $\hat{\theta} = RZ^\intercal(ZZ^\intercal)^{-1}$.

3. Experiments

3.1. Dataset

The proposed radiomic interpretation framework is evaluated on two datasets across three downstream tasks. The first dataset is a multi-study mpMRI collection from UCL hospital, including SmartTarget (Hamid et al., 2019), PICTURE (Simmons et al., 2018), ProRAFT (Orczyk et al., 2021), Index (Dickinson et al., 2013), PROMIS (Bosaily et al., 2015) and PROGENY (Linch et al., 2017). This dataset contains mpMRI from 850 patients, including T2-weighted image (T2), high-b value diffusion-weighted image (DWI), and Apparent Diffusion Coefficient (ADC) maps, with both lesion and prostate gland masks available on each T2 image. We refer to this dataset as the UCLH dataset in the following sections. The second dataset is consists of prostate mpMRI with the gland contour from $1,028$ patients recruited in the ReImagine Risk study (Marsden et al., 2021).

All images are resampled to voxel size of $0.5mm \times 0.5mm \times 1mm$. Each dataset is split into train, validation, and test set with a ratio of 7:1:2 on patient level, for downstream task fine-tuning and evaluation.

3.2. Foundation model pretraining

We adopt a recently released prostate mpMRI foundation model, ProFound, to investigate the fine-tuning effect. ProFound uses ConvNeXt v2 (Woo et al., 2023) and is pre-trained using masked autoencoder (MAE) (He et al., 2022), which is a self-supervised learning method that can be used to pre-train vision models. The model is pre-trained on an ensemble of private and public prostate mpMRI datasets of ~ 5000 patients, including the PI-CAI dataset (Saha et al., 2024), PROSTATE-MRI from the Cancer Imaging Archive (Choyke et al., 2025), the ReImagine Risk dataset (Marsden et al., 2021), and a private dataset (Min et al., 2025). More details such as pretraining protocols can be found at the ProFound repository [1].

3.3. Foundation model fine-tuning

To investigate the feature shift from fine-tuning the pre-trained foundation model, three prostate cancer related downstream tasks were explored.

Prostate cancer risk group classification. We fine-tune the ProFound model to predict the Prostate Imaging Reporting and Data System (PIRADS) scores, which is formulated as a multiclass classification task with patient groups of PIRADS scores of < 3, 3, 4, and 5. In this task, the ProFound model is fine-tuned by adding a simple head comprising two fully connected layers with an intermediate batch normalisation layer. The ReImagine risk dataset is used for the classification task and the model is trained with the Cross Entropy loss.

Prostate cancer lesion segmentation. The pre-trained model is adapted to delineate the lesion contour by inserting a UPerNet head (Xiao et al., 2018) after the encoder. Dice loss is used for fine-tuning the segmentation task on the UCLH dataset.

Prostate gland volume estimation. We also explore a regression task of predicting the prostate gland volume, where a simple head consisting of a batch normalisation layer

1. https://github.com/pipiwang/ProFound

followed by a fully connected layer is adopted. ProFound is fine-tuned on the UCLH dataset using the Mean Squared Error (MSE) loss.

All fine-tuned models are trained for 100 epochs with a learning rate of 0.001 using the AdamW optimiser. For the classification and segmentation task, the model takes input of three modalities, T2, high-b value DWI, and ADC maps, whereas the regression task only uses T2 as the model input.

3.4. Raiomic feature extraction

The radiomic features are extracted following a guidance (Zwanenburg et al., 2016) using PyRadiomics (ver 3.1.0) (Van Griethuysen et al., 2017) on all mpMRI modalities of each patient. A selection of features were extracted, including first-order features, Gray Level Co-occurrence Matrix (GLCM) features, Gray Level Size Zone Matrix (GLSZM) features, Gray Level Run Length Matrix (GLRLM) features, Neighbouring Gray Tone Difference Matrix (NGTDM) features, Gray Level Dependence Matrix (GLDM) features, from both original and Wavelet filtered images. The Min-Max normalisation is performed on each radiomic feature to scale all features to a range of $[0, 1]$. For the lesion segmentation task, we calculate two sets of radiomics, using lesion masks and prostate gland masks as ROIs respectively; while the prostate gland masks are used for the PIRADS score classification task and the prostate volume estimation task.

3.5. Training the shared non-linear mapping

To train the shared non-linear mapping f^{share} (in Sect.2.2), we perform a parameter sweep to decide the value of λ_1 and λ_2 over the combination of $\lambda_1 \in [0, 10^{-7}, 3 \times 10^{-7}, 10^{-6}, 3 \times 10^{-6}, 10^{-6}]$ and $\lambda_2 \in [0, 10^{-5}, 10^{-4}, 10^{-3}]$. The final adopted values are $\lambda_1 = 10^{-6}$ and $\lambda_2 = 10^{-5}$. The shared non-linear projection mapping is trained for 200 epochs with a learning rate of 0.001.

3.6. Representation shift measurement

To quantitatively measure the feature shift in representing radiomics after fine-tuning, we adopt the following metrics.

Importance score. For radiomic feature k of modality m, the importance is defined as $I_{m,k} = ||\theta_{m,k,:}||_2$. The change after fine-tuning is:

$$\Delta I_{m,k} = I^{ft}_{m,k} - I^{p}_{m,k}. \tag{6}$$

R^2 **score.** The R^2 score is also known as Coefficient of Determination, which is defined as

$$R^2 = 1 - \frac{Residual\ Sum\ of\ Squares}{Total\ Sum\ of\ Squares}. \tag{7}$$

We use R^2 to quantify how well the features from foundation model encoder describes the radiomics information.

Mean Squred Error. We also use MSE to investigate the capability of reconstructing radiomic features using the foundation model encoder representation.

4. Results

4.1. Quantitative performance of the interpretation framework

To assess the proposed radiomic feature representation framework, we report MSE and R^2 for three downstream tasks and various radiomic feature groups, as shown in Tab. 1. Higher MSE and lower R^2 were obtained after the foudnation model was adapted to specific tasks, suggesting that feature embeddings become less linearly recoverable into radiomic representations. A possible reason could be that fine-tuned encoder extracts more specialised information, whereas the self-supervise pre-trained model captures more general information about the input images.

Table 1: Quantitative results showing the performance of MLP across three downstream tasks on various group of features. CLS = classification task, REG = regression task, SEG-L = segmentation task with lesion mask as radiomics ROI, SEG-P = segmentation task with prostate gland mask as radiomics ROI

Feature	Stage	PIRADS CLS		Volume REG		Lesion SEG-L		Lesion SEG-P	
		MSE↓	R^2 ↑	MSE↓	R^2 ↑	MSE↓	R^2 ↑	MSE↓	R^2 ↑
First oder	Pre-train	0.437	0.584	0.263	0.727	0.722	0.344	0.703	0.351
	Fine-tune	0.452	0.569	0.366	0.621	0.775	0.296	0.732	0.325
GLCM	Pre-train	0.365	0.659	0.132	0.860	0.623	0.436	0.584	0.492
	Fine-tune	0.390	0.636	0.269	0.716	0.649	0.412	0.613	0.464
GLDM	Pre-train	0.326	0.697	0.162	0.826	0.625	0.440	0.593	0.468
	Fine-tune	0.347	0.669	0.260	0.719	0.771	0.307	0.620	0.442
GLRLM	Pre-train	0.263	0.760	0.140	0.851	0.656	0.422	0.725	0.367
	Fine-tune	0.331	0.698	0.227	0.760	0.812	0.272	0.746	0.348
GLSZM	Pre-train	0.614	0.409	0.453	0.529	0.928	0.186	0.752	0.272
	Fine-tune	0.631	0.393	0.577	0.399	1.006	0.116	0.787	0.238
NGTDM	Pre-train	0.287	0.735	0.103	0.892	0.712	0.361	0.665	0.400
	Fine-tune	0.300	0.717	0.206	0.785	0.838	0.263	0.735	0.336
Original	Pre-train	0.416	0.602	0.640	0.335	0.691	0.311	0.641	0.368
	Fine-tune	0.453	0.571	0.747	0.224	0.810	0.192	0.687	0.322
Wavelet	Pre-train	0.430	0.599	0.279	0.704	0.791	0.302	0.776	0.308
	Fine-tune	0.441	0.585	0.354	0.623	0.837	0.259	0.792	0.293

The regression performance on the classification and regression task operates on the prostate gland mask for radiomics calculation. For both downstream tasks, the radiomic representation model exhibits the lowest MSE and highest R^2 on NGTDM features with and without fine-tuning, indicating information about structural patterns or inflammation relevant markers (Aguirre-Meneses et al., 2025) being encoded by the foundation model. These patterns are likely to contribute more to the model predictive capability for PIRADS score classification and volume regression.

We evaluated the regression performance using radiomic features extracted from two ROI definitions, the lesion mask and the whole prostate gland. When radiomics were computed at the lesion level, the regression achieved low R^2, indicating that lesion-level features

provide limited explanatory power for the encoder representation in the segmentation task. This is likely due to the high variability and small spatial extent of individual lesions, which produce radiomic descriptors with low stability and weak correlation to global encoder embeddings. In contrast, using gland-level radiomics substantially improved the regression fit, yielding approximately $R^2 \approx 0.4$. This suggests that the encoder captures information more strongly aligned with global prostate characteristics than with fine-scale lesion appearance. Gland-level attributes such as organ size, zonal anatomy, and age-related tissue changes are known to correlate with cancer presence and localisation, which may explain their stronger correspondence with encoder features. These findings also imply that lesion-specific radiomic features may be too heterogeneous or insufficiently discriminative to establish a stable mapping for this task. For completeness and transparency, we report both ROI scenarios. Together, they illustrate that radiomics extracted at different anatomical scales provide different levels of explanatory value, and that the encoder's behaviour in lesion segmentation is more consistently reflected in global prostate characteristics than in local lesion descriptors.

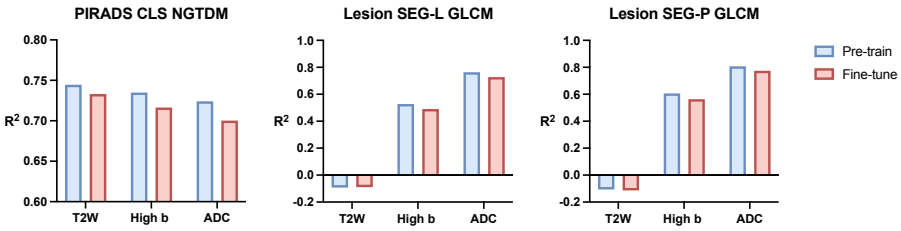

Figure 2: R^2 of single modality on mpMRI tasks on the highest overall R^2 features.

In addition to reporting radiomics group-wise performance, we also investigate the regression fit on different input modalities. We show three examples in Fig. 2, including the PIRADS classification task and the segmentation task with two ROI definition. Only the feature type with the highest R^2 after fine-tuning are illustrated as examples. It can be observed that in the PIRADS classification task, radiomics from all three modalities are aligned to the radiomic features to a substantial degree, indicating comparative predictive power of all modalities. While for the lesion segmentation task, high-b value DWI and ADC radiomics align with foundation model features while T2 bahaves the opposite, regardless of pre- or post- fine-tuning, which corresponds to the ability of ADC and high b DWI in identifying tumours by highlighting cancerous tissues with signal intensity different from normal tissues.

4.2. Qualitative case studies

To understand how fine-tuning reshapes the encoder representation for PIRADS prediction, we examined radiomic features whose ability to explain encoder embeddings changed the most, as shown in Fig. 3. For each radiomic descriptor, we quantified its explanatory value via ΔI calculated from before and after fine-tuning, then ranked features in three complementary ways: those that became newly important (positive ΔI), those whose importance

decreased (negative ΔI), and those with the least absolute change among features that were globally stable. These three views reveal how fine-tuning shifts the encoder toward radiologically meaningful image characteristics used in PIRADS scoring.

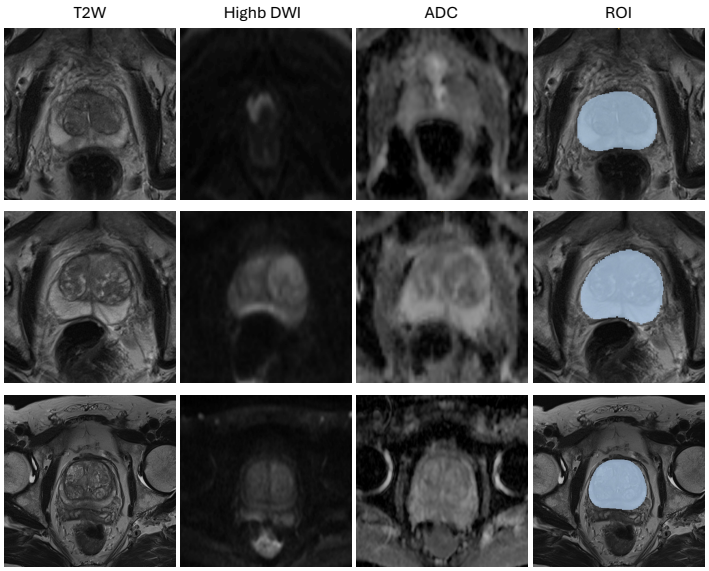

Top 5 positive relative ΔI

Modality	Feature type	Feature name
T2	GLCM	MCC
T2	GLCM	Correlation
T2	GLRLM	LongRunHighGrayLevelEmphasis
T2	GLRLM	LowGrayLevelRunEmphasis
T2	GLRLM	HighGrayLevelRunEmphasis

Top 5 negative relative ΔI

Modality	Feature type	Feature name
ADC	GLCM	Imc2
T2	GLRLM	ShortRunHighGrayLevelEmphasis
ADC	GLDM	DependenceNonUniformityNormalized
ADC	GLCM	DifferenceEntropy
highb	First order	Kurtosis

Lowest 5 absolute ΔI

Modality	Feature type	Feature name
ADC	First order	Total Energy
ADC	First order	Energy
T2	GLSZM	GrayLevelNonUniformityNormalized
T2	GLSZM	GrayLevelVariance
highb	First order	Maximum

Figure 3: Radiomic feature changes for PIRADS classification tasks. The left side shows patient cases with all modalities and the prostate gland ROI, and right side lists features with the top and least five ΔI.

Features gaining importance: increased alignment with T2 structural patterns. Radiomic features with the largest positive ΔI were predominantly T2-weighted texture and run-length measures, including GLCM-MCC, GLCM-correlation, and several GLRLM descriptors capturing long high-intensity runs or low-intensity structural streaks. These features quantify the coherence, organisation and zonal architecture of the prostate, for example in the peripheral and transition zones. PIRADS guidelines place strong emphasis on these T2 features, as lesion visibility and morphological distortion on T2-weighted imaging are central markers of clinical suspicion. The increased ability of these descriptors to explain the encoder after fine-tuning indicates that the model becomes more attuned to the structured appearance of malignant regions and to deviations from normal glandular texture patterns. This shift suggests that fine-tuning makes the encoder more aligned with radiologists' use of T2 structural cues for PIRADS assessment.

Features losing importance: reduced reliance on unstable diffusion heterogeneity. Radiomic features with the strongest negative ΔI primarily originated from ADC and high-b diffusion imaging. These include ADC-GLCM-Imc2, ADC-GLCM-DifferenceEntropy, ADC-GLDM-DNUN, and high-b kurtosis, all of which characterise fine-scale texture irregularity and local signal heterogeneity. While such patterns may loosely correlate with tumour presence, they are also known to be sensitive to acquisition noise, variation in b-values and small ROI instability, and they are not central to PIRADS scoring,

which emphasises consistent diffusion restriction rather than stochastic heterogeneity. The drop in explanatory power after fine-tuning suggests that the encoder moves away from these volatile cues, instead prioritising more robust diffusion features. This behaviour reflects the goal of fine-tuning: to refine the model toward radiologically reliable indicators of high PIRADS scores and to suppress spurious correlations.

Features with low shifts: stable global ADC and T2 indicators. Among radiomic features that explained a substantial portion of encoder variance both before and after fine-tuning, those with the lowest absolute changes while maintaining moderate to high importance score included global ADC intensity descriptors (TotalEnergy, Energy) and T2 gray-level distribution measures (GLSZM-GLNUN, GLSZM-Variance). These metrics quantify overall diffusion signal level and non-uniformity, as well as global heterogeneity across the gland. These are radiologically meaningful biomarkers: PIRADS scoring heavily relies on diffusion restriction (low ADC) and lesion conspicuity cross-correlated across T2 and diffusion sequences. These stable features correspond to fundamental anatomical or textural characteristics that provide contextual structure but are not strongly task-discriminative for PIRADS scoring.

Using our proposed approach, across all the analyses, fine-tuning produces a systematic, clinically interpretable reorganisation of encoder features. The encoder strengthens its alignment with zonal T2 textural structure, reduces sensitivity to noise-prone diffusion heterogeneity, and retains the weighting of global ADC/T2 intensity and non-uniformity—all of which mirror established criteria in PIRADS scoring. These results show that radiomics provides a meaningful, interpretable lens through which fine-tuning behaviour can be understood, demonstrating that the model becomes progressively more "radiologist-like" in the cues it uses to assess prostate cancer suspicion.

5. Conclusion

This study introduces a radiomics-based framework for interpreting how foundation model representations change during fine-tuning, offering a quantitative and clinically meaningful lens on encoder behaviour. Across three downstream prostate MRI tasks, we showed that radiomic features can partially reconstruct encoder embeddings, with the best alignment observed for, in particular, at gland-ROI-level radiomics and for modality–feature combinations consistent with radiological practice (e.g., high-b and ADC for lesion identification, global features for cancer risk). By comparing linear decoding weights before and after fine-tuning, our method revealed systematic and task-dependent shifts, for example increased sensitivity to zonal T2 structure for PIRADS prediction, reduced reliance on unstable diffusion heterogeneity and stable weighting of global ADC/T2 signal characteristics.

While the radiomics-to-latent mapping explains only a fraction of encoder variance, this limitation reflects the complementary nature of hand-crafted radiomics and high-capacity foundation models. Future work may explore richer interpretable feature spaces, non-linear or sparsity-aware decoding and cross-task comparisons to establish a broader taxonomy of fine-tuning-induced representation changes. Overall, our findings demonstrate that radiomics provides a practical and principled interpretability tool, enabling foundation models to be probed, compared, adapted and potentially better understood with greater transparency in medical imaging applications.

Acknowledgments

This work was supported by the National Institute for Health Research (NIHR) University College London Hospitals (UCLH) Biomedical Research Centre (BRC). This work was also supported by the International Alliance for Cancer Early Detection, an alliance between Cancer Research UK [C28070/A30912; C73666/A31378], Canary Center at Stanford University, the University of Cambridge, OHSU Knight Cancer Institute, University College London and the University of Manchester.

References

Heriberto Aguirre-Meneses, Pablo Stoehr-Muñoz, Mauricio Molina-Gonzalez, Marco-Antonio Nuñez-Gaona, Ernesto Roldan-Valadez, and Mauricio Molina-Gonzalez Sr. Radiomics and the image biomarker standardisation initiative (ibsi): A narrative review using a six-question map and implementation framework for reproducible imaging biomarkers. *Cureus*, 17(10), 2025.

A El-Shater Bosaily, C Parker, LC Brown, R Gabe, RG Hindley, R Kaplan, M Emberton, HU Ahmed, PROMIS Group, et al. Promis—prostate mr imaging study: a paired validating cohort study evaluating the role of multi-parametric mri in men with clinical suspicion of prostate cancer. *Contemporary clinical trials*, 42:26–40, 2015.

P Choyke, B Turkbey, M Merino, and B Wood, Jun 2025. URL http://doi.org/10.7937/K9/TCIA.2016.6046GUDv.

Louise Dickinson, Hashim U Ahmed, AP Kirkham, Clare Allen, Alex Freeman, Julie Barber, Richard G Hindley, Tom Leslie, Chloe Ogden, Rajendra Persad, et al. A multi-centre prospective development study evaluating focal therapy using high intensity focused ultrasound for localised prostate cancer: the index study. *Contemporary clinical trials*, 36 (1):68–80, 2013.

Yunguan Fu, Weixi Yi, Charlotte Manisty, Anish N Bhuva, Thomas A Treibel, James C Moon, Matthew J Clarkson, Rhodri Huw Davies, and Yipeng Hu. Cinema: A foundation model for cine cardiac mri. *arXiv preprint arXiv:2506.00679*, 2025.

Sami Hamid, Ian A Donaldson, Yipeng Hu, Rachael Rodell, Barbara Villarini, Ester Bonmati, Pamela Tranter, Shonit Punwani, Harbir S Sidhu, Sarah Willis, et al. The smart-target biopsy trial: a prospective, within-person randomised, blinded trial comparing the accuracy of visual-registration and magnetic resonance imaging/ultrasound image-fusion targeted biopsies for prostate cancer risk stratification. *European urology*, 75(5):733–740, 2019.

Kaiming He, Xinlei Chen, Saining Xie, Yanghao Li, Piotr Dollár, and Ross Girshick. Masked autoencoders are scalable vision learners. In *Proceedings of the IEEE/CVF conference on computer vision and pattern recognition*, pages 16000–16009, 2022.

M Linch, G Goh, C Hiley, Y Shanmugabavan, N McGranahan, A Rowan, YNS Wong, H King, A Furness, A Freeman, et al. Intratumoural evolutionary landscape of high-

risk prostate cancer: the progeny study of genomic and immune parameters. *Annals of Oncology*, 28(10):2472–2480, 2017.

Teresa Marsden, Hashim U Ahmed, and Mark Emberton. An update from the reimagine prostate cancer risk study (nct04060589): A prospective cohort study in men with a suspicion of prostate cancer who are referred onto a magnetic resonance imaging–based diagnostic pathway with donation of tissue, blood, and urine for biomarker analyses. *European Urology*, 80(4):398–399, 2021.

Niccolò McConnell, Pardeep Vasudev, Daisuke Yamada, Daryl Cheng, Mehran Azimbagirad, John McCabe, Shahab Aslani, Ahmed H Shahin, Yukun Zhou, Andre Altmann, et al. A computationally frugal open-source foundation model for thoracic disease detection in lung cancer screening programs. *arXiv preprint arXiv:2507.01881*, 2025.

Zhe Min, Fernando J Bianco, Qianye Yang, Wen Yan, Ziyi Shen, David Cohen, Rachael Rodell, Dean C Barratt, and Yipeng Hu. Segmentation versus detection: Development and evaluation of deep learning models for prostate imaging reporting and data system lesions localisation on bi-parametric prostate magnetic resonance imaging. *CAAI Transactions on Intelligence Technology*, 10(3):689–702, 2025.

Clement Orczyk, Dean Barratt, Chris Brew-Graves, Yi Peng Hu, Alex Freeman, Neil McCartan, Ingrid Potyka, Navin Ramachandran, Rachael Rodell, Norman R Williams, et al. Prostate radiofrequency focal ablation (proraft) trial: A prospective development study evaluating a bipolar radiofrequency device to treat prostate cancer. *The Journal of Urology*, 205(4):1090–1099, 2021.

Anindo Saha, Joeran S Bosma, Jasper J Twilt, Bram van Ginneken, Anders Bjartell, Anwar R Padhani, David Bonekamp, Geert Villeirs, Georg Salomon, Gianluca Giannarini, et al. Artificial intelligence and radiologists in prostate cancer detection on mri (pi-cai): an international, paired, non-inferiority, confirmatory study. *The Lancet Oncology*, 25(7): 879–887, 2024.

Lucy AM Simmons, Abi Kanthabalan, Manit Arya, Tim Briggs, Dean Barratt, Susan C Charman, Alex Freeman, David Hawkes, Yipeng Hu, Charles Jameson, et al. Accuracy of transperineal targeted prostate biopsies, visual estimation and image fusion in men needing repeat biopsy in the picture trial. *The Journal of urology*, 200(6):1227–1234, 2018.

Michal R Tomaszewski and Robert J Gillies. The biological meaning of radiomic features. *Radiology*, 298(3):505–516, 2021.

Joost JM Van Griethuysen, Andriy Fedorov, Chintan Parmar, Ahmed Hosny, Nicole Aucoin, Vivek Narayan, Regina GH Beets-Tan, Jean-Christophe Fillion-Robin, Steve Pieper, and Hugo JWL Aerts. Computational radiomics system to decode the radiographic phenotype. *Cancer research*, 77(21):e104–e107, 2017.

Sanghyun Woo, Shoubhik Debnath, Ronghang Hu, Xinlei Chen, Zhuang Liu, In So Kweon, and Saining Xie. Convnext v2: Co-designing and scaling convnets with masked autoen-

coders. In *Proceedings of the IEEE/CVF conference on computer vision and pattern recognition*, pages 16133–16142, 2023.

Chaoyi Wu, Xiaoman Zhang, Ya Zhang, Hui Hui, Yanfeng Wang, and Weidi Xie. Towards generalist foundation model for radiology by leveraging web-scale 2d&3d medical data. *Nature Communications*, 16(1):7866, 2025.

Tete Xiao, Yingcheng Liu, Bolei Zhou, Yuning Jiang, and Jian Sun. Unified perceptual parsing for scene understanding. In *Proceedings of the European conference on computer vision (ECCV)*, pages 418–434, 2018.

Kai Zhang, Rong Zhou, Eashan Adhikarla, Zhiling Yan, Yixin Liu, Jun Yu, Zhengliang Liu, Xun Chen, Brian D Davison, Hui Ren, et al. A generalist vision–language foundation model for diverse biomedical tasks. *Nature Medicine*, 30(11):3129–3141, 2024.

Yukun Zhou, Mark A Chia, Siegfried K Wagner, Murat S Ayhan, Dominic J Williamson, Robbert R Struyven, Timing Liu, Moucheng Xu, Mateo G Lozano, Peter Woodward-Court, et al. A foundation model for generalizable disease detection from retinal images. *Nature*, 622(7981):156–163, 2023.

Alex Zwanenburg, Stefan Leger, Martin Vallières, and Steffen Löck. Image biomarker standardisation initiative. *arXiv preprint arXiv:1612.07003*, 2016.